Synaptic plasticity with discrete state synapses

Henry D. I. Abarbanel*
Department of Physics and Marine Physical Laboratory (Scripps Institution of Oceanography) University of California, San Diego, La Jolla, CA 92093-0402, USA

Sachin S. Talathi†
Department of Physics and Institute for Nonlinear Science, University of California, San Diego, La Jolla, CA 92093-0402, USA

Leif Gibb
Graduate Program in Computational Neurobiology, Division of Biological Sciences, and Institute for Nonlinear Science, University of California, San Diego, La Jolla, CA 92093-0402, USA

M. I. Rabinovich
Institute for Nonlinear Science, University of California, San Diego, La Jolla, CA 92093-0402, USA
(Received 13 January 2005; revised manuscript received 1 June 2005; published 22 September 2005)

Experimental observations on synaptic plasticity at individual glutamatergic synapses from the CA3 Shaffer collateral pathway onto CA1 pyramidal cells in the hippocampus suggest that the transitions in synaptic strength occur among discrete levels at individual synapses [C. C. H. Petersen *et al.*, Proc. Natl. Acad. Sci. USA **85**, 4732 (1998); O'Connor, Wittenberg, and Wang, D. H. O'Connor *et al.*, Proc. Natl. Acad. Sci. USA (to be published); J. M. Montgomery and D. V. Madison, Trends Neurosci. **27**, 744 (2004)]. This happens for both long term potentiation (LTP) and long term depression (LTD) induction protocols. O'Connor, Wittenberg, and Wang have argued that three states would account for their observations on individual synapses in the CA3-CA1 pathway. We develop a quantitative model of this three-state system with transitions among the states determined by a competition between kinases and phosphatases shown by D. H. O'Connor *et al.*, to be determinant of LTP and LTD, respectively. Specific predictions for various plasticity protocols are given by coupling this description of discrete synaptic α-amino-3-hydroxy-5-methyl-4-isoxazolepropionic acid (AMPA) receptor ligand gated ion channel conductance changes to a model of postsynaptic membrane potential and associated intracellular calcium fluxes to yield the transition rates among the states. We then present various LTP and LTD induction protocols to the model system and report the resulting whole cell changes in AMPA conductance. We also examine the effect of our discrete state synaptic plasticity model on the synchronization of realistic oscillating neurons. We show that one-to-one synchronization is enhanced by the plasticity we discuss here and the presynaptic and postsynaptic oscillations are in phase. Synaptic strength saturates naturally in this model and does not require artificial upper or lower cutoffs, in contrast to earlier models of plasticity.

DOI: 10.1103/PhysRevE.72.031914 PACS number(s): 87.17.Aa, 87.16.Ac

I. INTRODUCTION

Experiments on synaptic plasticity at individual synapses in CA3 to CA1 hippocampal pathways reveal an "all-or-none" change in their synaptic strength [1,2]. Indications of this were seen a decade ago [C. F. Stevens and Y. Wang (personal communication)]. The recent measurements have given substantial standing to the notion that single synapses may operate as a discrete state system in their plastic changes associated with long-term potentiation (LTP) and long-term depression (LTD).

In this paper we first explore a general formulation of the possibility that individual synapses can express a finite number of discrete levels of conductance rather than the continuous or graded or analog picture often formulated [3–6]. Petersen *et al.* [1] have commented on the positive consequences for reliability of neural memory from discrete state synapses. In addition there is computational evidence for entry of a small number of free Ca^{2+} ions through volgate gated calcium channels and (N-methyl-D-aspartic acid) (NMDA) receptor ligand gated ion channel activated by synaptic stimulation during plasticity induction protocol [7]. A synapse which must respond to this very small signal might well select a strategy of an "all-or-none" response in adjusting its strength as a means of achieving a measure of reliability.

There are studies of network models using discrete state synapses [8] where the discreteness of the synaptic states is introduced as a useful computational device and not related to the observations of Petersen *et al.* [1] or others [9,10].

After a brief consideration of a general formulation of an L level synapse, we focus our attention on $L=3$, which is suggested by the recent data of Ref. [9]. With three levels we explore the transitions among the levels using observations of Ref. [9]. With some general arguments based on the measurements, we are able to establish values for the normalized

*Also at Institute for Nonlinear Science; University of California, San Diego, La Jolla, CA 92093-0402, USA.
†Electronic address: talathi@physics.ucsd.edu

conductances of the individual $L=3$ levels, and we suggest an experiment which will determine an interesting ratio among the transition rates. Montgomery and Madison [10] discuss the possibility of four discrete synaptic states, but it appears that because of the way they identify these states and the stability of one of the state, their identification may be equivalent to that of O'Conner, Wittenberg, and Wang [9].

The transition rates themselves depend on a model for how complex chemical pathways lead to the change in α-amino-3-hydroxy-5-methyl-4-isoxazolapropionic acid (AMPA) conductance and the number of AMPA receptors at any synapse [11–16]. We adopt a version of our earlier model [6] of these processes to provide a basis on which to make quantitative predictions of the outcome of various LTP and LTD induction protocols on the changes in AMPA conductance of a postsynaptic cell. We explore spike time-dependent protocols as well as presentation of spike bursts of various frequencies to the postsynaptic cell. These compare well to experiment, in particular to results presented in Wittenberg's dissertation [17], and predictions are made for various spike timing experiments.

We also explore the following setup: a periodically firing conductance based presynaptic neuron provides excitatory synaptic input to a periodically firing conductance based postsynaptic neuron. In certain ranges of frequency and conductance strength for the excitatory connection these neurons synchronize [18]. We explore the effect on this synchronization of our discrete synaptic strength model and show that the regime of one-to-one synchronization is significantly enlarged [19] for some conductance strengths and that the synchronization is an in-phase firing of the two neurons.

It is an important feature of models built on a finite number of discrete synaptic levels that the synaptic strength (AMPA conductance) is always bounded above and below. This is in contrast to models developed over the years, including our own [6,20], which do not have this property.

II. METHODS

A. Discrete state synapses: Transition rate models

The data of Ref. [9] suggest that three discrete states of AMPA conductance are found at individual synapses. If the total number of levels is L and they are indexed by $l=0,1,2,\ldots,L-1$, and there are N_S synapses indexed by $n=1,2,\ldots,N_S$, then we represent the occupation of synapse n in state l at time t by $N_l^n(t)$. These occupation numbers are either zero or unity. They can change in time due to LTP/LTD induction protocols or other biological processes. The average occupation number in state l is given by

$$p_l(t) = \frac{1}{N_S}\sum_{n=1}^{N_S} N_l^{(n)}(t). \tag{1}$$

These $p_l(t)$ will constitute the main dynamical variables of our model. They are taken to satisfy linear rate equations of the form

$$\frac{dp_l(t)}{dt} = \sum_{k=0}^{L-1}\{W_{(k\to l)}(t)p_k(t) - W_{(l\to k)}(t)p_l(t)\}. \tag{2}$$

The transition rates $W_{(k\to l)}(t), W_{(l\to k)}(t)$ are selected to assure

$$\sum_{k=0}^{L-1} p_k(t) = 1. \tag{3}$$

As long as the number of active synapses N_S is unchanged, this last equation follows from the definition of $p_k(t)$. In the limit of N_S large, we assume that the $p_l(t)$ remain finite; this is a standard assumption about such a limit for the description of a large number of objects each having a discrete set of states.

A statistical description of $N_S \gg 1$ independent synapses undergoing time dependent transitions among the allowed L states yields Eq. (1) on the average with fluctuations about this mean of order $1/\sqrt{N_S}$, as one might expect.

One can collect the average occupation numbers into an L-dimensional vector $\mathbf{P}(t)=(p_0(t),p_1(t),\ldots,p_{L-1}(t))$ which satisfies

$$\frac{d\mathbf{P}(t)}{dt} = \mathbf{M}(t)\cdot\mathbf{P}(t), \tag{4}$$

where $\mathbf{M}(t)$ is the $L\times L$ matrix of transition rates. The conservation rule (3) means that $\mathbf{M}(t)$ always has at least one zero eigenvalue [21,22]. The dynamics of $\mathbf{P}(t)$ takes place in the $(L-1)$-dimensional space orthogonal to the constant L-dimensional vector $\mathbf{C}=(1,1,1,\ldots,1)$.

The effect of having this constraint may be seen in the decomposition of $\mathbf{P}(t)=\mathbf{C}+\mathbf{P}_\perp(t)$, where $\mathbf{P}_\perp(t)\cdot\mathbf{C}=0$. The dynamics of motion for $\mathbf{P}_\perp(t)$ is

$$\frac{d\mathbf{P}_\perp(t)}{dt} = \mathbf{M}(t)\cdot\mathbf{P}_\perp(t) + \mathbf{M}(t)\cdot\mathbf{C}, \tag{5}$$

which is motion of the vector $\mathbf{P}_\perp(t)$ spanning the $(L-1)$-dimensional space orthogonal to $\mathbf{C}$ driven by the time-dependent forcing $\mathbf{M}(t)\cdot\mathbf{C}$. $\mathbf{P}_\perp(t)$ is defined up to a rotation about $\mathbf{C}$. This dynamical description is similar to that of driven precession of a spin in a time-dependent magnetic field.

Each discrete level $l=0,1,\ldots,L-1$ has a dimensionless AMPA conductance g_l normalized to some baseline. The dimensionless AMPA conductance of the neuron with N_S synapses is

$$G_{\mathrm{AMPA}}(t) = \sum_{n=1}^{N_S}\sum_{l=0}^{L-1} g_l N_l^n(t) = N_S\sum_{l=0}^{L-1} g_l p_l(t). \tag{6}$$

This means that the quantity

$$\frac{G_{\mathrm{AMPA}}(t)}{N_S} = \sum_{l=0}^{L-1} g_l p_l(t), \tag{7}$$

the normalized, dimensionless AMPA conductance per synapse, is independent of the number of synapses when N_S is large, depending only on the average occupation number of the synaptic levels and the conductance associated with each level. By definition of the baseline synaptic state, before any LTP/LTD induction protocols are presented to the postsynaptic neuron, this quantity is equal to 1:

$$\frac{G_{\mathrm{AMPA}}(t=0)}{N_S}=1. \tag{8}$$

In our work below, we report the quantity $G_{\mathrm{AMPA}}(t)/N_S-1$ as the output from our simulation of various induction protocols.

To fully specify the model of synaptic plasticity associated with the presence of discrete levels, we must identify the conductances g_l of each level, and, through some form of dynamics of the postsynaptic neuron, determine the transition rates. In the next section we do this for the suggested three state model of Ref. [9]. However, if observations indicate that there are $L\neq 3$ levels operating at some synapses, then the general formulation presented here will cover that situation as well.

B. Discrete state synaptic models

1. Two state model

In Refs. [2,9] there is clear evidence for a discrete two state system at individual synapses and measurements showing that the synapses appears to make sudden jumps between the two states. Yet in Ref. [9] there is presented evidence that when one presents a saturating LTD protcol followed by saturating LTP protocol, the LTD is fully reversible, while the opposite is not the case. We have chosen to investigate a three state synaptic model in this paper and include in the discussion the "locked-in" state called H^* by O'Conner, Wittenberg, and Wang [9]. Two state systems have been examined by Ref. [8], though not using the biophysical model for transitions between or among states developed here.

2. Three state model

If there are three states $l=0,1,2$ then we need to identify three discrete level conductances g_0,g_1,g_2 and the transition rates among the levels [9] call their three levels "low" (state 0 here), high (state 1 here), and "high locked-in" (state 2 here). They suggest that transitions associated with LTD protocols connect state 1 to state 0, and transitions associated with higher frequency protocols, typically leading to LTP, connect state 0 to state 1 and state 1 to state 2. They also note that when an LTD protocol is applied *following* a saturating LTP protocol to a population of synapses, the synapses cannot be depressed as fully as when the LTD protocol is applied to a naive population of synapses. The amount of depotentiation possible decreases over the 10 min following LTP induction. This led them to suggest the presence of a "high locked-in" state, called H^* by them; we call this state 2. They do not require transitions between state 2 and state 0 to account for their data, and we assume none as well.

Using these observations we associate an "LTD transition rate" $g(t)$ with the transition between state 1 and state 0. Similarly we associate an "LTP transition rate" $f(t)$ with transitions between state 0 and state 1. Loosely speaking we think of $g(t)$ as an aggregated action of phosphatases leading to the dephosphorylation and/or removal of synaptic AMPA receptors and $f(t)$ as the aggregated action of kinases operating in the opposite fashion [12,13]. In the next section we will specify how one evaluates these transition rates from a dynamical model of the postsynaptic neuron, but for the moment we note that f and g will depend on the elevation of intracellular postsynaptic calcium concentrations $[\mathrm{Ca}^{2+}]_i(t)$ above the equilibrium level $C_0\approx 100$ nM. Denoting the time course of postsynaptic intracellular calcium concentration as $C(t)=[\mathrm{Ca}^{2+}]_i(t)$, we define

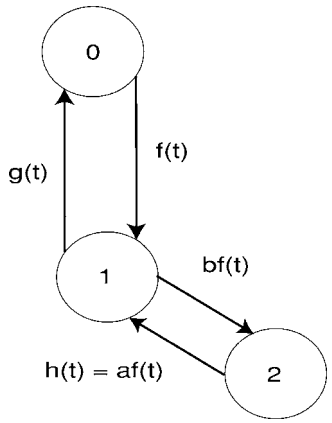

FIG. 1. Three state model of synaptic plasticity. Individual synapses can move among the three states, marked 0 for the "low" state, 1 for the "high" state, and 2 for the "high locked-in" state. The rules for state transition depend on the transition rates $f(t)$ and $g(t)$ governed by changes in intracellular calcium concentration. These transition rates are determined by LTP and LTD induction protocols.

$$\Delta C(t)=\frac{C(t)-C_0}{C_0}, \tag{9}$$

and the transition rates $f(t),g(t)$ are determined by $\Delta C(t)$ in a manner specified in the next section.

The transition between state 1 and the "high locked-in" state called 2 is taken to be proportional to the $0\rightarrow 1$ transition rate $f(t)$. If one had more detailed information on the biophysical kinase and phosphatase pathways, one could replace this simple assumption by a more complex quantity. We take this transition rate as $bf(t)$ with b a constant to be determined.

The picture outlined by Ref. [9] does not suggest a transition from state 2 to state 1, but we find it is necessary. For the moment we call this transition rate $h(t)$, and we will argue that it is proportional to $f(t)$. $h(t)$ cannot be zero, if the transition rate framework is to be consistent with observations associated with a "locked-in" state.

This discussion leads us to the transition rate (or "master") equations associated with the scheme depicted in Fig. 1:

$$\frac{dp_0(t)}{dt}=-f(t)p_0(t)+g(t)p_1(t),$$

$$\frac{dp_1(t)}{dt}=f(t)p_0(t)+h(t)p_2(t)-g(t)p_1(t)-bf(t)p_1(t),$$

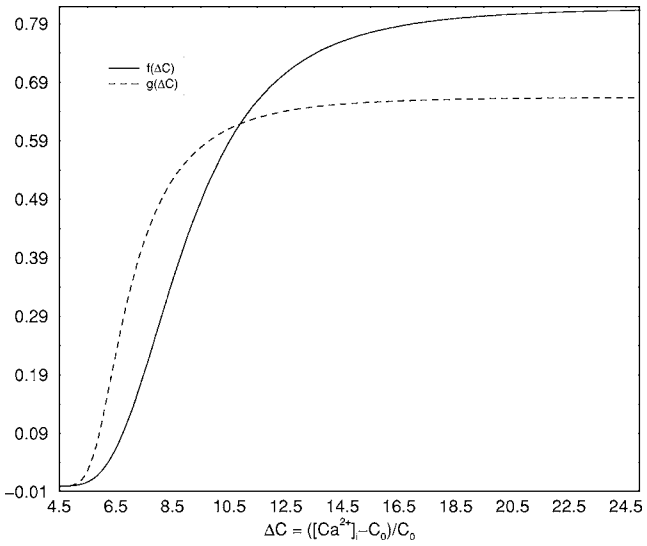

FIG. 2. Steady state values for the transition rates f and g plotted as function of the magnitude of the change in intracellular calcium concentration. ΔC is in arbitrary units. For small changes in intracellular calcium concentration only g is nonzero, corresponding to LTD induction, and for larger changes in intracellular calcium concentration, both f and g are nonzero with f being greater than g, corresponding to an LTP induction protocol.

$$\frac{dp_2(t)}{dt} = bf(t)p_1(t) - h(t)p_2(t). \tag{10}$$

By construction

$$\frac{d(p_0(t) + p_1(t) + p_2(t))}{dt} = 0. \tag{11}$$

Under prolonged stimulation the postsynaptic intracellular calcium levels reach approximately constant values, and we can ask what is the behavior of $\mathbf{P}(t)=(p_0(t),p_1(t),p_2(t))$ under such circumstances. This means the functions $f(t)$ and $g(t)$ are thought of now as constant in time with magnitude determined by the saturated level of $[Ca^{2+}]$. We associate this value of $\mathbf{P}$, after long constant $[Ca^{2+}]$ elevation, with the fixed point of the equations (10) for $\mathbf{P}(t)$. The state long after the induction protocol is completed will be the fixed point

$$\mathbf{P}_{\text{fixed point}} = \frac{(gh,fh,bf^2)}{h(f+g)+bf^2}. \tag{12}$$

In our models, low values of saturated intracellular calcium elevation ΔC are connected with LTD and higher values, with a competition between LTD and LTP [23]. The specific form of the connection between ΔC and f and g will be given shortly, but their general dependence is shown in Fig. 2 [24]. In an LTD protocol $g \neq 0$ but $f \approx 0$. In an LTP protocol both f and g may be nonzero.

If we take $h=ag$, then a saturating LTD protocol, with $g \neq 0$, $f \approx 0$, will deplete both states 1 and 2, leading to a final state $\mathbf{P}=(1,0,0)$. If, however, we apply a saturating LTP protocol where neither f nor g is zero, thus arriving at Eq. (12), and *then* apply a saturating LTD protocol, the choice $h=ag$ will lead us back to the state $\mathbf{P}=(1,0,0)$, which is not what is observed. Indeed, O'Connor *et al.* [9] note that the state reached by a saturating LTP protocol depotentiates to a state intermediate between all synapses in state 0 and the fully saturated state; namely, our fixed point (12).

If we choose $h=af$, then this saturating LTD protocol following the saturating LTP protocol leads us to

$$\mathbf{P} = \frac{(a(f+g),0,bf)}{a(f+g)+bf}, \tag{13}$$

namely, we depopulate state 1 due to the action of g. This is the kind of depotentiated, but not baseline, state seen by [9].

We conclude that the choice $h=af$ is consistent with the observations, and we cannot have $a=0$. If $a=0$, the high locked state would be totally populated by a strong LTP protocol and the synapse would not leave that state. Indeed, O'Connor *et al.* [9] indicate that after such a strong LTP protocol (two rounds of theta-burst stimulation), most but not all synapses, about 80%, are in state 2.

This completes the general formulation of the three level transition rate model. We now turn to the determination of the AMPA conductances g_l in each level $l=0,1,\ldots,L-1$ from the data presented by Ref. [9]. Then we discuss a conductance based neural model for the postsynaptic cell which permits us to translate electrophysiological activity into transition rates useful in the equations determining $\mathbf{P}(t)$.

C. Transition rates in a model for voltage and calcium dynamics

Evaluation of the transition rates f and g requires a specific model describing how the postsynaptic cell responds to various induction protocols presented either presynaptically or as paired presynaptic and postsynaptic actions. It also requires a model for the dynamics of Ca^{2+} in the postsynaptic cell. We proceed using the idea that changes in AMPA conductance are induced by the time course of elevation of intracellular Ca^{2+} [25–29]. The details of the pathways which follow elevation of Ca^{2+} are not specified in the phenomenological approach we use. In this regard we have explored both one and two compartment models of the voltage and intracellular calcium dynamics of a cell with AMPA receptors whose strength is changed as a result of biochemical pathways activated by the induction protocols. The two compartment model, which we utilize here, separates the cellular dynamics into a somatic compartment where action potentials are generated by the familiar sodium and potassium currents and a dendritic spine compartment where AMPA and NMDA receptors are located and intracellular calcium dynamics occurs. The details of this model are located in the Appendix to this paper. As one improves this model or replaces it with further experimental insights into the processes involved in LTP/LTD induction, one can use those improvements to provide evaluations for the transitions rates needed in the discrete state synapse model. Further exploration of the way postsynaptic Calcium elevation may influence AMPA strengths is found in Rubin *et al.* [30].

The output from the biophysical model of the neuron which we require in this section is focused on the time course of elevation of intracellular calcium concentration

relative to the equilibrium concentration $C_0 \approx 100$ nM. We call this time course $C(t)=[Ca^{2+}]_i(t)$ and seek the way in which

$$\Delta C(t) = \frac{C(t) - C_0}{C_0} \tag{14}$$

influences the transition rates $f(t), g(t)$.

Our model involves two auxiliary variables, $P(t)$ and $D(t)$, which satisfy first-order kinetics driven by Hill functions dependent on $\Delta C(t)$. These variables satisfy

$$\frac{dP(t)}{dt} = F_P[\Delta C(t)][1 - P(t)] - \frac{P(t)}{\tau_P}$$

$$\frac{dD(t)}{dt} = F_D[\Delta C(t)][1 - D(t)] - \frac{D(t)}{\tau_D}, \tag{15}$$

with driving terms

$$F_P(x) = \frac{\alpha_P x^L}{\xi_P^L + x^L}, \quad F_D(x) = \frac{\alpha_D x^M}{\xi_D^M + x^M}. \tag{16}$$

We used the constants $\tau_P=10$ ms, $\tau_D=30$ ms, $\alpha_p=1.0$, $\alpha_D=1.25$, $L=10.5$, $M=4.75$, $\xi_P=6.7$, and $\xi_D=13.5$ in our calculations for this work. These equations are discussed in our earlier paper [6].

These kinetic quantities are driven by elevation in Ca^{2+}, $\Delta Ca(t)>0$, from their resting value of zero. They are taken to be related to the transition rates as

$$f(t,\Delta C(t)) = P(t)D(t)^\eta,$$

$$g(t,\Delta C(t)) = P(t)^\eta D(t), \tag{17}$$

and $\eta=4$ as used in our earlier work. The quantities $f(t)$ and $g(t)$ have dimensions of frequency. Our arguments do not establish their magnitude but only provide a connection to their dependence on elevation of intracellular Ca^{2+} levels. Multiplying the relations here between $f(t)$ and $g(t)$ and $P(t)$ and $D(t)$ by a constant rescales the time while not affecting the final states which lead to specific statements of AMPA conductance changes after an induction protocol.

The model for voltage dynamics and Ca^{2+} dynamics is now established. To proceed we specify an electrophysiological protocol. For example we present a burst of spikes to the presynaptic terminal with an average interspike interval (ISI) of our choice. Our presynaptic terminal represents the population of terminals from presynaptic neurons onto a postsynaptic neuron. This induces a voltage and Ca^{2+} response in the postsynaptic cell, and from the time course of $\Delta C(t)$ we evaluate the transition rates $f(t)$ and $g(t)$. These enter the 'master' equation for the average occupations across the population of N_S synapses. Solving the equations for the $p_l(t)$ leads to our evaluation of

$$\frac{G_{\mathrm{AMPA}}(t)}{N_S} = g_0 p_0(t) + g_1 p_1(t) + g_2 p_2(t),$$

$$= 2 - \frac{4p_0(t)}{3}. \tag{18}$$

III. RESULTS

We first establish, using the measurements in [9] the values of the normalized, dimensionless AMPA conductances of the three levels at an individual synapse. Our arguments show that they are determined independently of the specific model for the transition rates. Then we develop a model for the transition rates which will allow us to make predictions about the response of the cells to various LTP and LTD protocols.

A. Determination of the discrete level conductances

At $t=0$ the observed average occupation of levels is observed to be $\mathbf{P}(0)=(\frac{3}{4},\frac{1}{4},0)$. This means the normalized AMPA conductance is

$$\frac{G_{\mathrm{AMPA}}(0)}{N_S} = 1 = \frac{3g_0}{4} + \frac{g_1}{4}. \tag{19}$$

If a strong, saturating LTD protocol is applied to this state, we reach $\mathbf{P}=(1,0,0)$, where the normalized AMPA conductance is g_0. It has been observed [9] that after the induction $G_{\mathrm{AMPA}}/N_S=0.65\pm0.03$. We take this to be $G_{\mathrm{AMPA}}/N_S=\frac{2}{3}=g_0$ which implies $g_1=2$.

Next apply a phosphatase blocker (okadaic acid was used in Ref. [9]) so $g=0$ and, as they did, present a saturating LTP signal to arrive at the state $\mathbf{P}=(0,af,bf)/(a+b)f=(0,a,b)/(a+b)$, which is independent of the transition rate f. This is precisely the fixed point noted above with $g=0$ and $h=af$. After this protocol, the normalized AMPA conductance is approximately 2, leading to

$$\frac{ag_1 + bg_2}{a+b} = 2, \tag{20}$$

and thus $g_2=2$. Our model corresponds to the set of normalized individual level conductances ($g_0=\frac{2}{3}$, $g_1=2$, $g_2=2$).

The constants a and b are not determined by the observations so far. Presumably they can be determined by applying various induction protocols once we have a model for the transition rates. The actual time series of

$$\frac{G_{\mathrm{AMPA}}(t)}{N_S} = \frac{2}{3}p_0(t) + 2p_1(t) + 2p_2(t) \tag{21}$$

will depend on a and b.

This ratio a/b can be determined by another experiment not yet conducted. Start with the naive synapse $\mathbf{P}(0)=(\frac{3}{4},\frac{1}{4},0)$, apply okadaic acid, so $g=0$ (as in Ref. [9]) which blocks phosphatases, and present a saturating LTP protocol. This leads to the state $\mathbf{P}=(0,a,b)/(a+b)$. Now wash out the okadaic acid and apply the kinase blocker k252a, setting $f=0$, and present a saturating LTD protocol. This leads one to the state $(a,0,b)/(a+b)$. The normalized AMPA conductance in this state is

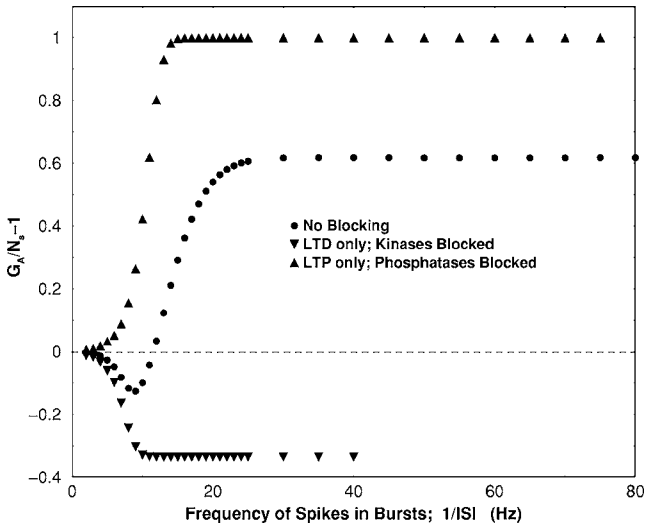

FIG. 3. Frequency-plasticity curve. The change in normalized AMPA conductance per synapse G_{AMPA}/N_s-1, is plotted as function of the frequency of a periodic burst of 10 presynaptic spikes presented to the presynaptic terminal. The circles represent synaptic plasticity for the full three state model. The upward-pointing triangles represent synaptic plasticity with the term $g(t)$ set to 0, corresponding to blocking phosphatase activity in the postsynaptic cell. One sees and expects LTP alone. The downward-pointing triangles represent the change in synaptic plasticity with the term $f(t)$ set to 0, corresponding to blocking kinase activity in the postsynaptic cell. We observe and expect LTD alone in this case. These results are quite similar to the observations of Ref. [9]

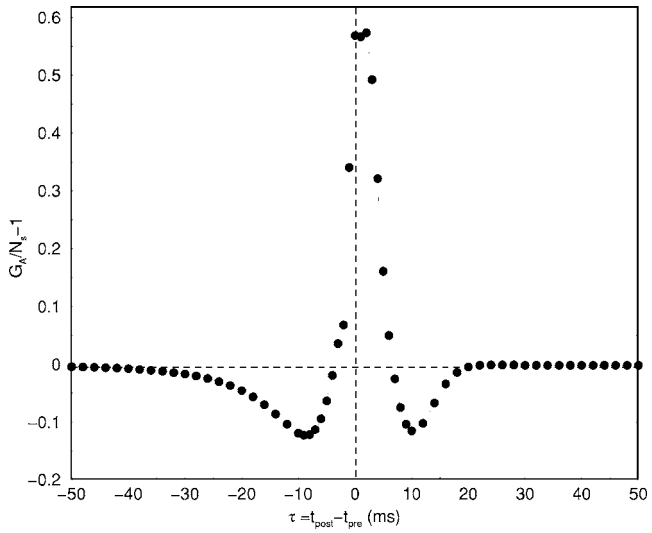

FIG. 4. Spike timing-dependent plasticity protocol. The change in normalized AMPA conductance per synapse G_{AMPA}/N_S-1, plotted as a function of the delay $\tau=t_{\mathrm{post}}-t_{\mathrm{pre}}$(ms), between presentation of a single presynaptic spike at t_{pre} and postsynaptic spike induced at t_{post}.

$$\frac{G_{\mathrm{AMPA}}}{N_S}=\frac{ag_0+bg_1}{a+b}=\frac{\frac{2}{3}\frac{a}{b}+2}{1+\frac{a}{b}}. \tag{22}$$

Measuring G_{AMPA}/N_S after this protocol sequence would give us a value for a/b.

B. LTP and LTD induction protocols

1. Presynaptic bursts

The first protocol we used presented a burst of ten spikes to the presynaptic terminal and evaluated $G_{\mathrm{AMPA}}(t)/N_S$ during and at the end of the induction period. The interspike interval (ISI) was constant in the burst, and we show in Fig. 3 the value of $G_{\mathrm{AMPA}}(t)/N_S-1$ after the burst as a function of frequency equal to 1/ISI. Three calculations are presented. The first, shown with filled circles, involves the action of both the LTP inducing transition rate $f(t)$ and the LTD inducing transition rate $g(t)$. As in the experimental data there is a region of no change in AMPA conductance per synapse for very low frequencies, then a region of LTD until this crosses into a region of persistent LTP. The second calculation, shown with upright triangles, removes the LTD inducing transition rate, so $g(t)=0$, which is achieved by Ref. [9] by the use of okadaic acid. In this calculation we see that LTP alone is induced at all frequencies where there is a measurable effect. The maximum AMPA conductance in the present model is $G_{\mathrm{AMPA}}(t)/N_S=2$ occurring when the lowest state is totally depleted. The value of unity for $G_{\mathrm{AMPA}}(t)/N_S-1$ is expected when a saturating LTP protocol is applied. Finally, a third result shown in Fig. 3 is the set of points with inverted triangles which occur when one blocks kinase action, again following the experimental procedures of Ref. [9], which means $f(t)=0$ in our language. Here we see a persistent LTD dropping to $G_{\mathrm{AMPA}}(t)/N_S-1\approx-\frac{1}{3}$ above frequencies of 10 Hz. This is the smallest possible value in the present model, as with this induction protocol and $f(t)=0$ the lowest state is fully populated, and the AMPA conductance, in dimensionless, normalized units is $\frac{2}{3}$.

All of this is consistent with the observations and the expectation of saturating LTP and LTD protocols in the discrete state plasticity model we have developed. It is important to note that the bounded nature of the AMPA conductance is quite important as in many other models, including our own [4–6], there is no guarantee that $G_{\mathrm{AMPA}}(t)/N_S$ is bounded above or below.

2. Spike timing plasticity

The exploration of spike timing-dependent plasticity at hippocampal synapses has resulted from the investigations of the phenomenon since the work of Refs. [31,32], Poo and his colleagues [33–35], and Feldman [36] over the past few years. We explored this in the present model by first presenting a spike presynaptically at a time t_{pre} and evoking a postsynaptic spike at t_{post}. The change $G_{\mathrm{AMPA}}(t)/N_S-1$ is a function only of $\tau=t_{\mathrm{post}}-t_{\mathrm{pre}}$ and for our model is shown in Fig. 4. This reproduces the characteristic window of LTP centered near $\tau=0$ and of width $\approx$10 ms around this point. Also shown in Fig. 4 are the LTD regions on both sides of this window. The one for τ negative is seen in many experiments. The LTD region for τ positive has been seen in ex-

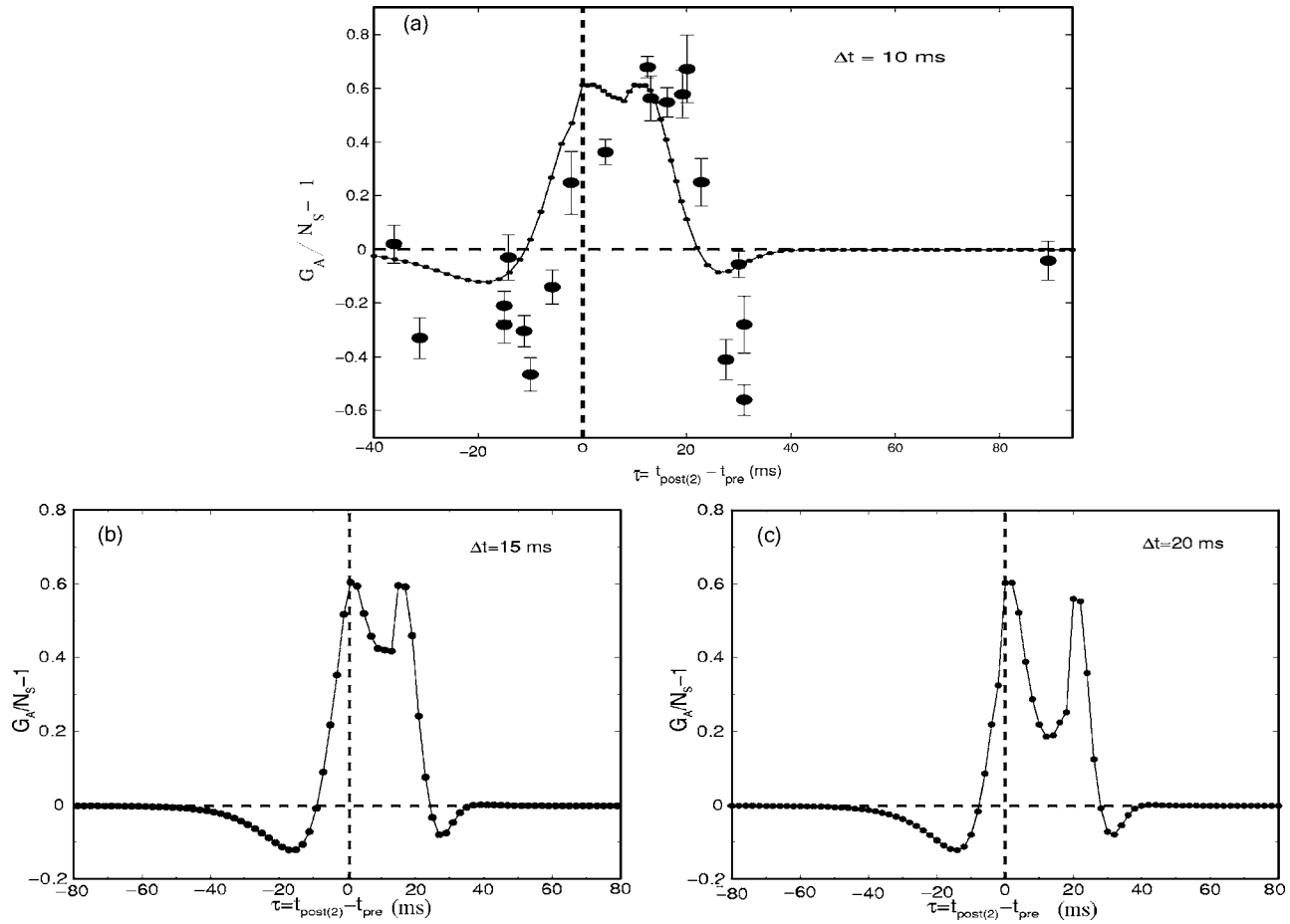

FIG. 5. (a) Change in normalized synaptic strength as a function of the delay $\tau=t_{post(2)}-t_{pre}$ when a single presynaptic spike is paired with two postsynaptic spikes 10 ms apart. $t_{post(2)}$ is the time of the second postsynaptic spike. Model results (points connected by lines) are plotted with experimental data of G. M. Wittenberg (large filled circles with error bars; Wittenberg 2003 [17], used with permission). Normalized synaptic strength, for the model, is the normalized AMPA conductance per synapse (G_{AMPA}/N_S) after the pairing. For the experiments, it is the average peak excitatory postsynaptic current (EPSC) height measured 10–20 min after the end of the pairing protocol, normalized by the mean baseline peak EPSC height (error bars: standard error of the mean). In the experiments, pairing was repeated 100 times at 5 Hz. (b) Here we plot change in normalized synaptic strength as a function of the delay $\tau=t_{post(2)}-t_{pre}$ when a single presynaptic spike is paired with two postsynaptic spikes 15 ms apart. As in case (a), we see a distinct dip in potentiated AMPA conductance is observed for times when presynaptic spike falls in between the two postsynaptic spike presentations. (c) Similar plot of change in normalized synaptic strength as a function of the delay $\tau=t_{post(2)}-t_{pre}$ when a single presynaptic spike is paired with two postsynaptic spikes 20 ms apart.

periments reported by Ref. [34], and it is common in models, including ours, which focus on postsynaptic intracellular Ca^{2+} as inducing the chain of events leading to AMPA plasticity.

Nishiyama *et al.* [34] used cesium instead of potassium in the intracellular pipette solution, and this has been argued by Wittenberg [17] to depolarize the postsynaptic cell and broaden the action potential artificially. To address this, Wittenberg has performed experiments in which this additional depolarizing effect is mimicked by presenting a spike timing protocol with one presynaptic spike at time t_{pre} and *two* postsynaptic spikes with a time difference Δt. She uses $\Delta t = 10$ ms, and the outcome of this protocol for our model is plotted in Fig. 5(a) with the experimental data [17] (used with permission). The change in normalized synaptic strength resulting from this protocol (G_{AMPA}/N_S-1 for the model) is shown as a function of the time of the second postsynaptic spike $t_{post(2)}-t_{pre}$. For the experiments, normalized synaptic strength is the average peak excitatory postsynaptic current (EPSC) height measured 10–20 min. after the end of the pairing protocol, normalized by the mean baseline peak EPSC height. It is clear that the LTP window is substantially larger than when we evoke just one postsynaptic spike and resembles the experimental data. We can regard this as a prediction of our discrete state plasticity model. Further predictions of this protocol are shown in Figs. 5(b) and 5(c), where $\Delta t=15$ ms and $\Delta t=20$ ms, respectively. In each case there is a distinct LTD window for positive $t_{post(2)}-t_{pre}$ and a distinctive dip between the LTP peaks whose separation is dictated by Δt.

Our model exhibits a number of features of LTP and LTD observed experimentally at CA3-CA1 synapses, including trapping of synapses in a high-strength state, separability of potentiation and depression by simulated inhibition of kinase

or phosphatase activity, and spike timing-dependent plasticity [9,17]. However, there are a number of ways in which the model can be developed further. For example, using the protocols of Ref. [9], population LTP at CA3-CA1 synapses rises gradually to a peak level over a few minutes; LTD takes a few minutes longer than this to develop fully. Our model does not yet include such a long timescale, but could be modified phenomenologically to do so. The authors of Ref. [9] have also found that the high locked-in state in populations of synapses builds up over several minutes. To model this phenomenon, we would again need to include a longer time scale.

While the spike timing-dependent plasticity induced in our model by 1 presynaptic and 2 postsynaptic spikes is similar to that observed by Ref. [17], our result for 1 presynaptic and 1 postsynaptic spike appears to differ from experimental observations [G. M. Wittenberg and S. S.-H. Wang (unpublished), data quoted with the authors' permission]. In particular, they observed little LTP but significant LTD near $t_{\text{post}}-t_{\text{pre}}=0$. At other values of $t_{\text{post}}-t_{\text{pre}}$, they observed only LTD. This suggests that such a protocol provides insufficient postsynaptic Ca^{2+} influx to induce LTP reliably. In contrast, our model shows a narrow but clear window of LTP centered near $t_{\text{post}}-t_{\text{pre}}=0$. At these values of $t_{\text{post}}-t_{\text{pre}}$, the Ca^{2+} influx in our model is sufficient to give f a relatively large value and thus induce LTP. If the data of Wittenberg and Wang are correct, then our model will need to be adjusted so that this Ca^{2+} influx is not sufficient to induce LTP.

In addition, the model can be used to explore the results of various LTP and LTD induction protocols that we have not simulated here but that are used by Ref. [9] and others in their experiments, such as theta burst stimulation and pairing protocols. In the long term, a model that more accurately describes the postsynaptic signaling pathways will eventually account for all of these various features of the data in a biologically satisfying manner.

C. Synchronization of two periodic neural oscillators with discrete state synapses

The final consequence we have investigated of our discrete state plasticity model is for the synchronization of oscillating neurons. We take as given that synchronization among populations of neurons can play an important role in their performing important functional activity in biological neural networks. We have abstracted the synchronous activity of populations of neurons to the simplest setup: two periodically oscillating Hodgkin-Huxley (HH) neurons coupled by a synaptic current which we explore with and without plastic synapses.

We have selected the postsynaptic neuron to be our two compartment model as described in the Appendix and set it into autonomous oscillations with a period T_2^0. This period is a function of the injected dc current into the somatic compartment. We hold this fixed while we inject a synaptic AMPA current

$$I_{\text{synapse}}(t) = g_{\text{AMPA}}(t)S_A(t)[E_{\text{rev}} - V_{\text{post}}(t)], \tag{23}$$

into the postsynaptic somatic compartment. $V_{\text{post}}(t)$ is the membrane voltage of this postsynaptic compartment.

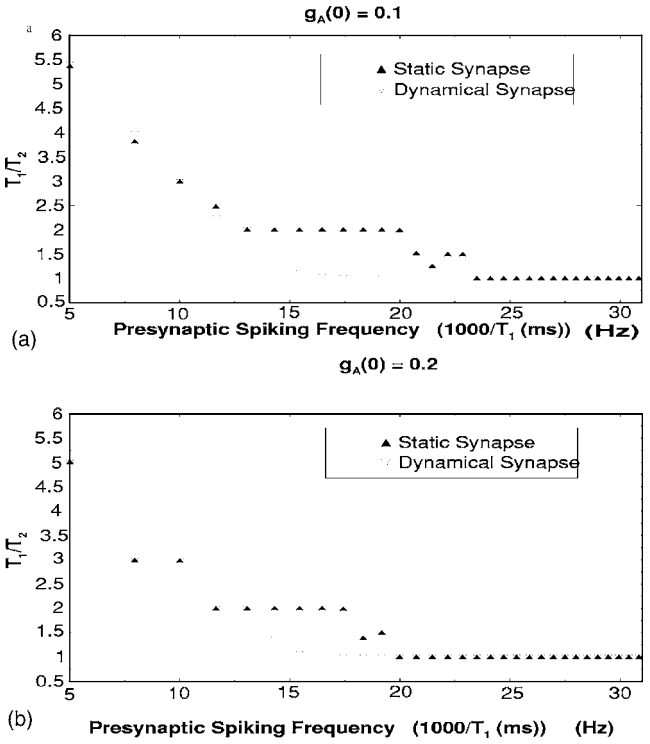

FIG. 6. (a) T_1/T_2, the ratio of the interspike interval T_1 of the presynaptic neuron to the interspike interval T_2 of the postsynaptic neuron, is plotted as a function of the presynaptic input frequency $1000/T_1$ Hz for a synapse starting at a base AMPA conductance of $g_{\text{AMPA}}(t=0)=0.1$ mS/cm^2. We see that the one-to-one synchronization window is broadened when the static synapse is replaced by a plastic synapse as determined by the three state model. (b) A similar plot for different value of base AMPA strength $g_{\text{AMPA}}(t=0)=0.2$ mS/cm^2.

$g_{\text{AMPA}}(t)$ is our time-dependent maximal AMPA conductance, and $S_A(t)$ satisfies

$$\frac{dS_A(t)}{dt} = \frac{1}{\tau_A}\frac{S_0(V_{\text{pre}}(t)) - S_A(t)}{S_{1A} - S_0(V_{\text{pre}}(t))} \tag{24}$$

as described in detail in the Appendix. $V_{\text{pre}}(t)$ is the periodic presynaptic voltage which we adjust by selecting the injected dc current into the presynaptic HH neuron. We call the period of this oscillation T_1.

When $g_{\text{AMPA}}=0$ the neurons are disconnected and oscillate autonomously. When $g_{\text{AMPA}}(t)\neq 0$ the synaptic current into the postsynaptic neuron changes its period of oscillation from the autonomous T_2^0 to the driven value of T_2, which we evaluate for various choices of T_1. We expect from general arguments [37] that there will be regimes of synchronization where T_1/T_2 equal integers and half-integers over the range of frequencies $1/T_1$ presented presynaptically. This will be true both for fixed g_{AMPA} and when $g_{\text{AMPA}}(t)$ varies as determined by our model.

In Fig. 6(a) we present T_1/T_2 as function of the frequency $1000/T_1$ (T_1 is given in milliseconds, so this is in units of Hz) for fixed $g_{\text{AMPA}}=0.1$ mS/cm^2 and for $g_{\text{AMPA}}(t)=g_{\text{AMPA}}[g_{\text{AMPA}}(t)/N_S]$ determined from our model. This

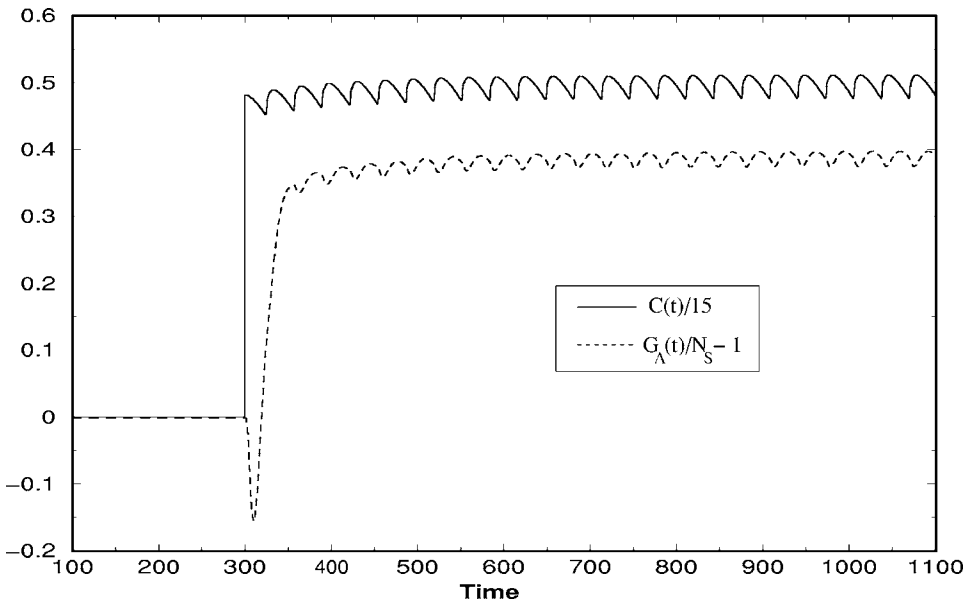

FIG. 7. Intracellular calcium concentration, scaled by 15, and the change in normalized synaptic strength $G_{\mathrm{AMPA}}(t)/N_S-1$, is plotted as a function of time in the case when a periodically spiking postsynaptic cell is driven by a periodically spiking presynaptic input.

value is what we used in our earlier calculations with the two compartment model. It amounts to a choice for the baseline value of the AMPA conductance. The fixed g_{AMPA} results are in filled upright triangles and, as expected, show a regime of one-to-one synchronization over a range of frequencies. One also sees regions of two-to-one and hints of five-to-two and three-to-one synchronization. These are expected from general arguments on the parametric driving of a nonlinear oscillator by periodic forces.

When we allow g_{AMPA} to change in time according to the model we have discussed above, we see (unfilled inverted triangles) a substantial increase in the regime of one-to-one synchronization, the appearance of some instances of three-to-two synchronization, and a much smaller regime with two-to-one synchronization. This suggests that the one-to-one synchronization of oscillating neurons, which is what one usually means by neural synchrony, is substantially enhanced when the synaptic coupling between neurons is allowed to vary by the rules we have described.

We show the same results in Fig. 6(b) for $g_{\mathrm{AMPA}}=0.2\ \mathrm{mS/cm^2}$. The fixed coupling is larger leading to stronger synchronization of the two neurons in a one-to-one manner even for fixed coupling. Here too (inverted, unfilled triangles) we see that allowing g_{AMPA} to vary in time enlarges the regime of one-to-one synchronization.

In Figs. 7 and 8 we explore aspects of the internal dynamics of plasticity and Ca^{2+} time courses for these results. In Fig. 7 we show $C(t)=[Ca^{2+}]_i(t)$ (scaled by a factor of 15 to fit on this graphic) and $G_{\mathrm{AMPA}}(t)/N_S-1$ in response to a presentation of periodic presynaptic oscillations beginning at a time 300. As noted earlier, the timescales for the intracellular Ca^{2+} processes and the timing in changes in $G_{\mathrm{AMPA}}(t)$ are not determined by our model. An arbitrary constant can multiply the definitions of the transitions rates $f(t)$ and $g(t)$. Both quantities rapidly rise, after a small transient of LTD, to positive but oscillating levels. The maximum $G_{\mathrm{AMPA}}(t)/N_S-1$ is 1 in our model, and we see that this saturating level is not reached in this protocol.

Finally, in Fig. 8 we examine how the synchronization manifests itself in the postsynaptic somatic and dendritic compartment membrane potentials. We plot these potentials along with $V_{\mathrm{pre}}(t)$. It is clear that the one-to-one synchronization occurs with an in-phase oscillation of the presynaptic and postsynaptic cells. The very short time delay between the somatic and dendritic compartments of the postsynaptic neuron is part of the model dynamics and not associated with the presentation of periodic presynaptic spikes to the postsynaptic cell. The in-phase synchronization is not seen in other, less biophysically based, models of plastic synapses and represents a very desirable feature of this model.

IV. DISCUSSION

The observations, recent and over the years, of discrete levels for synaptic strength at individual synapses in the

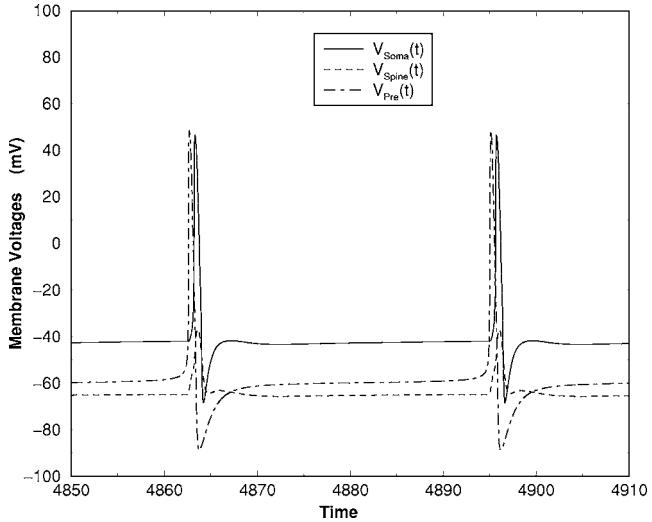

FIG. 8. $V_{\mathrm{soma}}(t)$, $V_{\mathrm{dendrite}}(t)$, and $V_{\mathrm{pre}}(t)$, plotted as functions of time, when the presynaptic and postsynaptic neurons are synchronized. Note that the presynaptic and postsynaptic neurons are synchronized in-phase with an internal $V_{\mathrm{soma}}(t)$ to $V_{\mathrm{spine}}(t)$, time difference determined by the two compartments of the model neuron.

CA3-CA1 hippocampal pathways represents a fundamental property important for the ways we learn and remember. There is a very interesting and important biophysical question about the mechanisms which lead to the expression of a few discrete levels of AMPA conductance at which individual synapses may be found. We do not address this fundamental question in this paper, but we have used the observation to construct a model based on discrete levels with transition rates among the levels determined by biophysical dynamics.

We have formulated a discrete level synaptic system in a general way with L levels allowed to the AMPA conductance, and then, following the observations of Ref. [9] we specialized to $L=3$. The dynamical variables in our model when $L=3$ are the average occupation numbers of each level $\mathbf{P}(t)=(p_0(t),p_1(t),p_2(t))$. These are averages over a collection of N_S synapses which contribute to the overall AMPA determined response of the neuron. While each individual synapse resides in one of three discrete states, so the individual occupation numbers at any given synapse are either zero or one, the average occupation numbers are smoothly varying, subject only to $p_0(t)+p_1(t)+p_2(t)=1$, by definition.

We developed differential equations for $\mathbf{P}(t)$ which are linear in the $p_l(t)$, $l=0,1,2$

$$\frac{dp_l(t)}{dt}=\sum_{l'=0}^{2} M_{ll'}p_{l'}(t), \tag{25}$$

and where the transition rates $M_{ll'}$ are determined by nonlinear membrane voltage and intracellular Ca^{2+} dynamics.

From the observations of Ref. [9] we argued that the transition rates shown in Fig. 1 sufficed to explain their measurements, and using their reported results we were able to determine that the conductances of the three individual levels in normalized, dimensionless units were $g_0=\frac{2}{3}$, $g_1=2$, $g_2=2$. The time dependence of the normalized, dimensionless AMPA conductance per synapse is then

$$\frac{G_{\mathrm{AMPA}}(t)}{N_S}=\sum_{l=0}^{2} p_l(t)g_l=2-\frac{4p_0(t)}{3}. \tag{26}$$

Using our values for the g_l and a dynamical model of the transition rates $f(t),g(t)$ as shown in Fig. 1, we reproduced the observed plasticity in response to a burst of presynaptic spikes with interspike intervals (ISIs) over the observed range. Further we made predictions for the response of this model to spike timing plasticity both for one presynaptic and one postsynaptic spike and for the case of two postsynaptic spikes evoked Δt apart accompanied by one presynaptic spike. We presented our results for $\Delta t=10$, 15, and 20 ms.

Finally we examined the dynamical role played by this discrete state plasticity model in the synchronization of two periodically oscillating Hodgkin-Huxley neurons. One such neuron oscillating with period T_2^0 was driven by another such neuron with period T_1. The final period T_2 of the driven neuron, relative to T_1, was plotted against $1/T_1$ and showed familiar regions of synchronization. For fixed AMPA coupling $g_{\mathrm{AMPA}}=G_{\mathrm{AMPA}}/N_S$ we found synchronization over some range of $1/T_1$ and then demonstrated that allowing g_{AMPA} to vary according to the plasticity model resulted in a much larger regime of one-to-one synchronization with the two neurons oscillating in phase. The results for synchronization have not been tested experimentally, though some experiments using dynamic clamp based synapses have been performed [20].

One striking aspect of the discrete state model, certainly not limited to our own work, is that the AMPA conductance has natural upper and lower bounds. Many other models of plasticity, including our own, do not share this important feature.

Some of our results, in particular the strengths of the normalized, dimensionless conductances of the synaptic levels are dependent primarily on the data of Ref. [9]. All of the transition rates are determined by our two compartment model for the neuron, as presented in the text and in the Appendix.

This model will change over time and be improved by further understanding of the biophysical processes leading to the discrete states and their transitions among themselves. The general framework we have presented describing how the three observed states are connected and several general results about that system will remain as the representation of the transition rates is improved.

While our model is based on the idea of discrete state synapses, by design it describes only populations of such synapses. In future work we plan to address this discreteness at the level of single synapses and small numbers of synapses. Questions of interest would include the following. (1) When the number of synapses is small, does the spread in the experimental data from trial to trial on excitation of individual synapses correspond the the fluctuations observed in our model over many trials? (2) Is there evidence for heterosynaptic interaction? Our model arises when we taken $N_S \gg 1$ independent synapses undergoing essentially the same trainsitions and average over the synapses. If their is interaction among synapses, this would need to be modified, and it is likely that in the examination of the dynamics of a few synapses, rather than the many studied here, we will be able to develop an understanding of interactions among synapses. In Nishiyama *et al.* [34] there is evidence for heterosynaptic interactions via calcium dynamics, perhaps mediated by the endoplasmic reticulum. (3) What is the role, when the number of synapses is small, of the probabilistic nature of presynaptic vesicle release? We have passed over these interesting issues in this paper while focusing on the whole cell behavior.

The dynamics of discrete state synapses is likely to be most interesting when placed in a network context. What new phenomena will arise when the synaptic strengths are bounded below and above while working in a network with learning is yet to be explored. We have made some preliminary calculations with the discrete state model when it is used in our earlier description of the role of plasticity in maintaining adult birdsong [38]. The indications are that the important fixed point in that investigation is retained while the runaway behvior seen there is "cured." However, it is clear that there is much yet to explore in this regard.

ACKNOWLEDGMENTS

This work was partially funded by the U.S. Department of Energy, Office of Basic Energy Sciences, Division of Engineering and Geosciences, under Grants No. DE-FG03-90ER14138 and DE-FG03-96ER14592; by the National Science Foundation Grant No. NSF PHY0097134, and from the National Institutes of Health Grant No. NIH R01 NS40110-01A2. Two of us (H.A. and S.S.T.) are partially supported by the NSF sponsored Center for Theoretical Biological Physics at UCSD. We have had many productive conversations with S. S.-H. Wang about the data from his laboratory, and we appreciate the comments he has made on the model presented. Permission to use results from the Ph.D. dissertation of Gail Wittenberg is also much appreciated.

APPENDIX

In this Appendix we give the details of the two compartment model of the postsynaptic neuron used in our calculations. The somatic compartment is the site of spike generation by the familiar Hodgkin-Huxley (HH) Na^+, K^+, and leak currents. The dendritic spine compartment has these currents as well as a voltage gated calcium current and glutamate driven NMDA and AMPA channels. The Ca^{2+} dynamics in the dendritic compartment drives the synaptic plasticity, namely changes in the AMPA conductance.

1. The somatic compartment

The dynamical equation for the somatic compartment takes the general form

$$C_M\frac{dV_S(t)}{dt} = I_{\mathrm{Na}}(V_S(t),t) + I_{\mathrm{K}}(V_S(t),t) + I_L(t) + I_{S\mathrm{dc}} + I_S(t) + G_{S\leftarrow D}[V_D(t) - V_S(t)]. \tag{A1}$$

The currents I_{Na}, I_{K}, I_L, are the familiar HH Na^+, K^+, and leak currents. $I_{S\mathrm{dc}}$ is a dc current used to set the resting potential of the cell. $I_S(t)$ is an externally managed time dependent current injected into the somatic compartment. It allows us to evoke an action potential at a specific time in the somatic compartment. This propagates back to the dendritic compartment to induce a depolarizing effect. $G_{S\leftarrow D}(V_D(t) - V_S(t))$ represents the current flowing into the somatic compartment from the dendritic compartment. It couples the voltages of the somatic and dendritic compartments. C_M is the membrane capacitance.

The value of the currents I_{Na}, I_{K}, and I_L are determined as usual with

$$I_L(t) = g_L[E_L - V_S(t)], \tag{A2}$$

where g_L is the conductance of the leak current and E_L is the reversal potential. The voltage gated currents are described by

$$I(V,t) = \bar{g}g(t,V)(E_{\mathrm{eq}} - V), \tag{A3}$$

where E_{eq} is the reversal potential and $\bar{g}$ is the maximal conductance. Both these values are fixed. The value of $g(t,V)$, the fraction of open channels, on the other hand, depends on the membrane potential and time.

In the case of channels in which $g(t,V)$ changes, the value of $g(t,V)$ depends on the state of "gating particles" $m(t,V)$ and $h(t,V)$, where $m(t,V)$ is the activation gate and $h(t,V)$ represents the inactivation gate. If N is the number of activation gates, and M, the number of inactivation gates then

$$g(t,V) = m(t,V)^N h(t,V)^M.$$

The state of the gating particles, given by $m(t,V)$ or $h(t,V)$, is a function of the membrane potential as well as time.

These gating variables, denoted by $X(t)$, are taken to satisfy first order kinetics:

$$\frac{dX(t)}{dt} = \frac{X_0(V(t)) - X(t)}{\tau_X(V(t))} = \alpha_X(V(t))(1 - X(t)) - \beta_X(V(t))X(t). \tag{A4}$$

From the standard HH model, we have the following relations for the conductances of the Na^+ and K^+ currents.

$$g_{\mathrm{Na}}(V,t) = m(V,t)^3 h(V,t),$$

$$g_{\mathrm{K}}(V,t) = n(V,t)^4,$$

where $m(V,t), n(V,t)$ are activation gating particles and $h(V,t)$ represents the inactivation gating particle. At the end of this appendix we give the functions X_0, τ_X, or $\alpha_X(V), \beta_X(V)$ for each of the voltage gated ionic currents, in addition to listing all the model parameters used in the simulations.

2. The dendritic compartment

The dynamics of the dendritic compartment membrane potential is given by

$$C_M\frac{dV_D(t)}{dt} = I_{\mathrm{Na}}(V_D(t),t) + I_{\mathrm{K}}(V_D(t),t) + I_L(V_D(t)) + I_A(V_D(t),t) + I_M(V_D(t),t) + I_{D\mathrm{dc}} + I_{\mathrm{AMPA}}(t) + I_{\mathrm{NMDA}}(t) + I_{\mathrm{VGCC}}(t) + G_{D\leftarrow S}[V_S(t) - V_D(t)]. \tag{A5}$$

$I_{D\mathrm{dc}}$ is a dc current used to set the resting potential of the cell. I_{Na}, I_{K}, and I_L represent the standard HH ionic and leak currents used in the somatic compartment as described above. In addition to these ionic currents we have considered two additional K^+ currents I_A and I_M. I_A currents have been reported to modulate the width of action potentials and influence the excitability of the cell. In our model, I_A attenuates the dendritic action potential, which is evoked by backpropagation of the somatic action potential.

The gating equations for I_M and I_A are

$$g_M(t,V) = u(t,V)^2,$$

$$g_A(t,V) = a(t,V)b(t,V),$$

where $u(t,V)$ and $a(t,V)$ are activation gating particles and $b(t,V)$ represents an inactivation gating particle.

As mentioned above all ionic currents in the dendritic compartment are also given in terms of Ohm's law (A3). Again $G_{D\leftarrow S}[V_S(t)-V_D(t)]$ represents current flowing into the dendritic compartment through the somatic compartment.

In addition to the currents mentioned above we have three other currents critical to the synaptic plasticity discussed here. There is a current associated with the ligand gated NMDA receptors (NMDARs). The form for this is

$$I_{\mathrm{NMDA}}(t) = g_{\mathrm{NMDA}} S_N(t) B(V_D(t))[V_{\mathrm{NMDA\text{-}eq}} - V_D(t)]$$

where g_{NMDA} is the maximal conductance associated with the channel. $S_N(t)$ ranges between zero and unity, representing the percentage of open channels at any time. To achieve the time course of this process in NMDARs, we use a two component form for S_N,

$$S_N(t) = w_f S_{N1}(t) + (1 - w_f) S_{N2}(t), \tag{A6}$$

$0 \leqslant w_f \leqslant 1$, and where $S_{Nl}(t), l=1,2$ satisfies

$$\frac{dS_{Nl}(t)}{dt} = \frac{1}{\tau_{Nl}} \frac{S_0(V_{\mathrm{pre}}(t)) - S_{Nl}(t)}{S_{1Nl} - S_0(V_{\mathrm{pre}}(t))}. \tag{A7}$$

V_{pre} is scaled to lie between 0 and 1 as it represents the arrival of an action potential at the presynaptic terminal. Its function is in turn to release neurotransmitter.

$S_0(V_{\mathrm{pre}}(t))$ is a step function which rises sharply from 0 to 1 when neurotransmitter is released as a result of the presynaptic action potential. When this occurs $S_{Nl}(t)$ rises from zero towards unity with a time constant $\tau_{Nl}(S_{1Nl}-1)$. When the effect of presynaptic action is completed, $S_{Nl}(t)$ relaxes towards zero with a time constant $\tau_{Nl}S_{1Nl}$. w_f represents the fraction of fast NMDA component contribution to NMDA current. In our model we have chosen $w_f=0.81$, $\tau_{N1}=67.5$, $S_{1N1}=70/67.5$, $\tau_{N2}=245$, $S_{1N2}=250/245$. In addition the conductance of the NMDA current depends on postsynaptic voltage via the term $B(V)$ whose form is given as

$$B(V) = \frac{1}{1 + 0.288[\mathrm{Mg}^{2+}]e^{-0.062V}}, \tag{A8}$$

where the concentration of magnesium is in mM and the voltage is in mV. For simulation purposes we have taken the physiologically reasonable value of $\mathrm{Mg}^{2+}=1$ mM.

This voltage-dependent conductance depends on the extracellular magnesium concentration. The voltage dependence of the current is mediated by the magnesium ion which, under normal conditions, blocks the channel. The cell must therefore be sufficiently depolarized to remove the magnesium block. Finally for this excitatory channel $V_{\mathrm{NMDA\text{-}eq}} \approx 0$ mV.

I_{AMPA} represents the ligand gated AMPA receptor current. This is taken to be of the form

$$I_{\mathrm{AMPA}} = g_{\mathrm{AMPA}} S_A(t)[V_{\mathrm{AMPA-eq}} - V_D(t)], \tag{A9}$$

where g_{AMPA} is the maximal conductance for this channel and $S_A(t)$ is the percentage of open channels, satisfying

$$\frac{dS_A(t)}{dt} = \frac{1}{\tau_A} \frac{S_0(V_{\mathrm{pre}}(t)) - S_A(t)}{S_{1A} - S_0(V_{\mathrm{pre}}(t))}. \tag{A10}$$

Again the rise time is less than a millisecond. In our formulation this time is $\tau_A(S_{1A}-1)$, which we set to 0.1 ms. AMPA currents decay in approximately 1–3 ms. In our formulation this decay time is $\tau_A S_{1A}$, which we set to 1.5 ms. We also take $V_{\mathrm{AMPA-eq}}=0$ mV.

The final and very important ingredient in inducing synaptic plasticity is the voltage gated calcium channel (VGCC). We have used the low threshold current I_T for this. The current from this channel takes the form

$$I_{\mathrm{VGCC}}(t) = g_C G(V(t)) m_c^2(t) h_c(t), \tag{A11}$$

where g_C is the maximal conductance of this channel, $m_c(t)$ is the activation function, and $h_c(t)$ is the inactivation function. $G(V)$ is the Goldman-Hodgkin-Katz function

$$\begin{aligned} G(V) &= -\frac{V}{C_0} \frac{[\mathrm{Ca}^{2+}]_i(t) - [\mathrm{Ca}^{2+}]_o e^{-2VF/RT}}{1 - e^{-2VF/RT}} \\ &= -\frac{V}{C_0} \frac{C(t) - [\mathrm{Ca}^{2+}]_o e^{-2VF/RT}}{1 - e^{-2VF/RT}}, \end{aligned} \tag{A12}$$

where $C(t)=[\mathrm{Ca}^{2+}]_i(t)$. The Goldman-Hodgkin-Katz function is used because of the large disparity in the intracellular $[\mathrm{Ca}^{2+}]_i$ and the extracellular $[\mathrm{Ca}^{2+}]_o$ concentrations. F is Faraday's constant, R is the gas constant, and T the absolute temperature. Other factors of the $G(V)$ equation are absorbed in the conductance g_C. C_0 is the equilibrium intracellular $[\mathrm{Ca}^{2+}]$ concentration, which is about 100 nM.

3. Coupling between the somatic and dendritic compartments

The coupling parameters between the two compartments are determined from the cytoplasmic resistance and the metric dimensions of each compartment. We take the specific cytoplasmic resistance of the cell to be $r_i=200\ \Omega$ cm.

We take the somatic compartment to be a isopotential sphere of $d_{\mathrm{soma}}=32.5\ \mu$m in diameter and the dendritic compartment to be an isopotential cylinder of diameter $d_{\mathrm{dendrite}}=10\ \mu$m and length $l_{\mathrm{dendrite}}=360\ \mu$m.

In order to determine the coupling resistance value we assume the somatic compartment to be a cylinder of equivalent surface area. We then have the total cytoplasmic resistance of the somatic compartment

$$R_{I\mathrm{soma}} = \frac{r_i l_{\mathrm{soma}}}{X(A_{\mathrm{soma}})} = 0.007839 \times 10^7 \Omega$$

while the total cytoplasmic resistance for the dendritic compartment is

$$R_{I\mathrm{dendrite}} = \frac{r_i l_{\mathrm{dendrite}}}{X(A_{\mathrm{den}})} = 1.713 \times 10^7 \Omega,$$

where $X(A_{\mathrm{soma}}) = \pi d_{\mathrm{soma}}^2/4.0$, and $X(A_{\mathrm{den}}) = \pi d_{\mathrm{dendrite}}^2/4.0$. Therefore, the average cytoplasmic coupling resistance

$$R_I = \frac{R_{I\text{soma}} + R_{I\text{dendrite}}}{2} \approx \frac{R_{I\text{dendrite}}}{2} = 0.861 \times 10^7 \Omega.$$

The coupling parameters in units of mS/cm^2 are calculated as

$$G_{S\leftarrow D} = \frac{1}{A_{\text{soma}} R_I} = 3.5 \text{ mS/cm}^2 \tag{A13}$$

and

$$G_{D\leftarrow S} = \frac{1}{A_{\text{den}} R_I} = 1.0 \text{ mS/cm}^2 \tag{A14}$$

4. Calcium dynamics

The dynamics of intracellular calcium $[Ca^{2+}]_i(t)$ in the dendritic compartment, which affects the efficacy of synaptic strength, is comprised of $[Ca^{2+}]_i(t)$ decaying to an equilibrium value of C_o on a timescale of $\tau_C \approx 15$ ms, which we take to be about 30 ms in our model, plus fluxes of $[Ca^{2+}]_i(t)$ due to the three channels, AMPA, NMDA, and VGCC considered in the dendrite model above. The first-order differential equation for $[Ca^{2+}]_i(t) = C(t)$ then is

$$\frac{dC(t)}{dt} = \frac{1}{\tau_C}[C_o - C(t)] + C_{\text{NMDA}} + C_{\text{AMPA}} + C_{\text{VGCC}}, \tag{A15}$$

where

$$C_{\text{NMDA}} = g_{\text{NC}} S_N(t) B(V_D(t))[V_{\text{NMDA-eq}} - V_D(t)],$$

$$C_{\text{AMPA}} = g_{\text{ac}} S_A(t)[V_{\text{NMDA-eq}} - V_D(t)],$$

$$C_{\text{VGCC}} = g_{\text{CC}} G(V_D(t)) m_c^2(t) h_c(t).$$

The constants $g_{\text{NC}}, g_{\text{ac}}, g_{\text{CC}}$ are not the same, even dimensionally, as the conductances in the voltage equation. Their values, given at the end if this appendix, reflect among other things, that the net AMPA current is composed primarily of other ions in addition to Ca^{2+} and that NMDA channels are highly permeable to Ca^{2+} ions. This completes the description of our model.

5. Parameters in the two compartment model

The various constants appearing in our two compartment model are collected here. The membrane capacitance is $C_M = 1.0\ \mu\text{F/cm}^2$ for all neurons.

The somatic compartment. The maximal conductances, in units of mS/cm^2, of the ionic currents are $g_{\text{Na}} = 215$, $g_{\text{K}} = 43$, $g_L = 0.813$. The reversal potentials in units of mV are $V_{\text{Na-eq}} = 50$, $V_{\text{K-eq}} = -95$, and $V_{L\text{-eq}} = -64$. The dc current injected into the somatic compartment $I_{S\text{dc}} = -7.0\ \mu\text{A/cm}^2$, so that the cell is at -75 mV at rest. The magnitude of the additional current injected into the somatic compartment is $I_{\text{soma}} = 160.8\ \mu\text{A/cm}^2$; in using it to induce a postsynaptic spike, it is taken to have a duration of 1 ms or less. $C_M = 1.0\ \mu\text{F/cm}^2$.

The dendritic compartment. For the standard HH ionic currents we have the same parameters as above. Maximal conductances associated with various dendritic currents, in units of mS/cm^2, are $g_{\text{NMDA}} = 0.05$, $g_{\text{AMPA}} = 1.75$, and $g_C = 1. \times 10^{-6}$. In the Mg^{2+} blockage function $B(V)$, we take $[Mg^{2+}] = 1$ mM. In the GHK function $G(V)$, the ratio of external $[Ca^{2+}]$ to equilibrium intracellular $[Ca^{2+}]$ is 15 000. The temperature is 25 °C. The conductance values for additional potassium currents used are $g_M = 6.7$ and $g_A = 100$ in units of mS/cm^2. Finally, $I_{D\text{dc}} = -7.0\ \mu\text{A/cm}^2$. $C_M = 1.0\ \mu\text{F/cm}^2$.

Calcium dynamics. For calcium dynamics we have $\tau_C = 30$ ms, $g_{\text{NC}} = 0.15$, $g_{\text{ac}} = 1.5 \times 10^{-5}$, and $g_{\text{CC}} = 3.5 \times 10^{-5}$. These are in units of $\text{mV}^{-1}\ \text{ms}^{-1}$. C_0, the basal calcium concentration in the cell, is normalized to 1.

Finally in the equation for the NMDA and AMPA channel open percentages $S_N(t)$ and $S_A(t)$, we use the "step" function

$$S_0(V) = \tfrac{1}{2}\{1 + \tanh[120(V - 0.1)]\}$$

and the constants $\tau_A = 1.4$ ms, $\tau_{N\text{fast}} = 67.5$ ms, $\tau_{N\text{slow}} = 245.0$ ms, $S_{1A} = \frac{15}{14}$, $S_{1N\text{fast}} = \frac{70}{67.5}$, $S_{1N\text{slow}} = \frac{250}{245}$.

6. Activation and deactivation parameters of various channels

$$\alpha_m(V) = \frac{0.32[13 - (V - V_{\text{th}})]}{e^{[13-(V-V_{\text{th}})]/4.0} - 1},$$

$$\beta_m(V) = \frac{0.28[(V - V_{\text{th}}) - 40]}{e^{[(V-V_{\text{th}})-40]/5} - 1},$$

$$\alpha_h(V) = 0.128 e^{17-(V-V_{\text{th}})/18},\ \beta_h(V) = \frac{4}{e^{40-(V-V_{\text{th}})/5} + 1},$$

$$\alpha_n(V) = \frac{0.032[15 - (V - V_{\text{th}})]}{e^{[15-(V-V_{\text{th}})]/5} - 1},\ \beta_n(V) = \frac{0.5}{e^{(V-V_{\text{th}})-10/40}},$$

$$m_{co}(V) = \frac{1}{1 + e^{-(52+V)/6.2}},$$

$$\tau_{mc}(V) = 0.204 + \frac{0.333}{e^{-(131+V)/16.7} + e^{(15+V)/18.2}},$$

$$h_{co}(V) = \frac{1}{1 + e^{(72+V)/4}},\ \alpha_u(V) = \frac{0.016}{e^{-(V+52.7)/23}},$$

$$\beta_u(V) = \frac{0.016}{e^{(V+52.7)/18.8}},\ \alpha_a(V) = \frac{-0.05(V + 20)}{e^{-V+20/15} - 1},$$

$$\beta_a(V) = \frac{0.1(V + 10)}{e^{(V+10)/8} - 1},\ \alpha_b(V) = \frac{0.00015}{e^{(V+18)/15}},$$

$$\beta_b(V) = \frac{0.06}{e^{-(V+73)/12} + 1},$$

$$\tau_{hc}(V) = 0.333e^{(V+466)/66.6} \text{ if } V \leqslant -81,$$

$$= 9.32 + 0.333e^{-(V+21)/10.5} \text{ if } V > -81,$$

where Vth$=-65$ mV in the soma compartment and -48 mV in the dendrite compartment.

7. Numerical method

All the simulations for the model presented in this work were written in C and used a fourth-order Runge-Kutta algorithm with a fixed time step of 0.01 ms. They were run under Linux on a computer with an Athlon 2400 MHz processor.

8. Code for the model

The code for the model can be obtained from http://inls.ucsd.edu/~talathi/Wangcode/Code.tar.gz.

[1] C. C. H. Petersen, R. C. Malenka, R. A. Nicoll, and J. J. Hopfield, Proc. Natl. Acad. Sci. U.S.A. **95**, 4732 (1998).
[2] D. H. O'Connor, G. M. Wittenberg, and S. S.-H. Wang, Proc. Natl. Acad. Sci. U.S.A. (to be published).
[3] G. C. Castellani, E. M. Quinlan, L. N. Cooper, and H. Z. Shouval, Proc. Natl. Acad. Sci. U.S.A. **98**, 12 772 (2001).
[4] U. R. Karmarkar and D. V. Buonomano, J. Neurophysiol. **88**, 507, 2001.
[5] H. Z. Shouval, M. F. Bear, and L. N. Cooper, Proc. Natl. Acad. Sci. U.S.A. **99**, 10 831 (2002).
[6] H. D. I. Abarbanel, L. Gibb, R. Huerta, and M. I. Rabinovich, Biol. Cybern. **89**, 214 (2003).
[7] K. M. Franks and T. J. Sejnowski, BioEssays **24**, 1130 (2002).
[8] P. Del Giudice, S. Fusi, and M. Mattila, J. Physiol. (Paris) **97**, 659 (2003).
[9] D. H. O'Connor, G. M. Wittenberg, and S. S.-H. Wang, J. Pulp Pap. Sci. (to be published).
[10] J. M. Montgomery and D. V. Madison, Trends Neurosci. **27**, 744 (2004); Neuron **33**, 765 (2002).
[11] R. C. Carroll, D. V. Lissin, M. Zastrow, R. A. Nicoll, and R. C. Malenka, Nat. Neurosci. **2**, 454 (1999).
[12] J. Lisman, H. Schulman, and H. Cline, Nat. Rev. Neurosci. **3**, 175 (2002).
[13] D. G. Winder and D. J. Sweatt, Nat. Rev. Neurosci. **2**, 461 (2001).
[14] A. Contractor and S. F. Heinemann, Sci. STKE **156**, RE14 (2002).
[15] R. Malinow and R. C. Malenka, Annu. Rev. Neurosci. **25**, 103 (2002).
[16] M. Sheng and M. J. Kim, Science **298**, 776 (2002).
[17] G. M. Wittenberg, Ph.D. thesis, Princeton University, Princeton, NJ, 2003.
[18] A. Pikovsky, M. Rosenblum, and J. Kurths, *Synchronization, a Universal Concept in Nonlinear Sciences* (Cambridge University Press, Cambridge, 2001).
[19] V. P. Zhigulin, M. I. Rabinovich, R. Huerta, and H. D. I. Abarbanel, Phys. Rev. E **67**, 021901 (2003).
[20] T. Nowotny, V. P. Zhigulin, A. I. Selverston, H. D. I. Abarbanel, and M. I. Rabinovich J. Neurosci. **23**, 9776 (2003).
[21] G. Lawler, *Introduction to Stochastic Processes*, Chapman and Hall Probability Series, 1st ed. (Chapman and Hall, London, 1995).
[22] N. G. Van Kampen, *Stochastic Processes in Physics and Chemistry*, 2nd ed. (Elsevier Science Publishers, Amsterdam, 1992).
[23] S. N. Yang, Y. G. Tang, and R. S. Zucker, J. Neurophysiol. **81**, 781 (1999).
[24] J. M. Bradshaw, Y. Kubota, T. Meyer, and H. Schulman, Proc. Natl. Acad. Sci. U.S.A. **100**, 10512 (2003).
[25] A. Artola and W. Singer, Trends Neurosci. **16**, 480 (1993).
[26] R. C. Malenka and R. A. Nicoll, Science **285**, 1870 (1999).
[27] B. L. Sabatini, M. Maravall, and K. Svoboda, Curr. Opin. Neurobiol. **11**, 349 (2001).
[28] P. J. Sjöstrom and S. B. Nelson, Curr. Opin. Neurobiol. **12**, 305 (2002).
[29] T. R. Soderling and V. A. Derkach, Trends Neurosci. **23**, 75, (2000).
[30] J. E. Rubin, R. C. Gerkin, G.-Q. Bi, and C. C. Chow, J. Neurophysiol. (to be published).
[31] D. Debanne, B. H. Gahwiler, and S. M. Thompson, Proc. Natl. Acad. Sci. U.S.A. **91**, 1148 (1994).
[32] H. Markram, J. Lubke, J. Frotscher, and B. Sakmann, Science **275**, 213 (1997).
[33] G. Q. Bi and M.-M. Poo, J. Neurosci. **18**, 10 464 (1998).
[34] M. Nishiyama, K. Hong, K. Mikoshiba, M.-M. Poo, and K. Kato, Nature (London) **408**, 584 (2000).
[35] G. Q. Bi and M. M. Poo, Annu. Rev. Neurosci. **24**, 139 (2001).
[36] D. E. Feldman, Neuron **27**, 45 (2000).
[37] P. G. Drazin, *Nonlinear Systems* (Cambridge University Press, Cambridge, 1992).
[38] H. D. I. Abarbanel, S. S. Talathi, G. Mindlin, L. Gibb, and M. I. Rabinovich, Phys. Rev. E **70**, 051911 (2004).